Three-Dimensional Electronic Structure of the Type-II Weyl Semimetal WTe_2

Domenico Di Sante,[1,*] Pranab Kumar Das,[2,3,†] C. Bigi,[4] Z. Ergönenc,[5] N. Gürtler,[5] J. A. Krieger,[6,7] T. Schmitt,[8] M. N. Ali,[9] G. Rossi,[4] R. Thomale,[1] C. Franchini,[5] S. Picozzi,[10] J. Fujii,[2] V. N. Strocov,[8] G. Sangiovanni,[1] I. Vobornik,[2] R. J. Cava,[9] and G. Panaccione[2]

[1]*Institut für Theoretische Physik und Astrophysik, Universität Würzburg, Am Hubland Campus Süd, Würzburg 97074, Germany*
[2]*Istituto Officina dei Materiali (IOM)-CNR, Laboratorio TASC, in Area Science Park, S.S.14, Km 163.5, I-34149 Trieste, Italy*
[3]*International Centre for Theoretical Physics (ICTP), Strada Costiera 11, I-34100 Trieste, Italy*
[4]*Dipartimento di Fisica, Universitá di Milano, Via Celoria 16, I-20133 Milano, Italy*
[5]*Computational Materials Physics, University of Vienna, Sensengasse 8/8, A-1090 Vienna, Austria*
[6]*Laboratory for Muon-Spin Spectroscopy, Paul Scherrer Institute, CH-5232 Villigen, Switzerland*
[7]*Laboratorium für Festkörperphysik, ETH-Hönggerberg, CH-8093 Zürich, Switzerland*
[8]*Paul Scherrer Institute, Swiss Light Source, CH-5232 Villigen, Switzerland*
[9]*Department of Chemistry, Princeton University, Princeton, New Jersey 08544, USA*
[10]*Consiglio Nazionale delle Ricerche (CNR-SPIN), Via Vetoio, L'Aquila 67100, Italy*

(Received 17 February 2017; published 14 July 2017)

By combining bulk sensitive soft-x-ray angular-resolved photoemission spectroscopy and first-principles calculations we explored the bulk electron states of WTe_2, a candidate type-II Weyl semimetal featuring a large nonsaturating magnetoresistance. Despite the layered geometry suggesting a two-dimensional electronic structure, we directly observe a three-dimensional electronic dispersion. We report a band dispersion in the reciprocal direction perpendicular to the layers, implying that electrons can also travel coherently when crossing from one layer to the other. The measured Fermi surface is characterized by two well-separated electron and hole pockets at either side of the Γ point, differently from previous more surface sensitive angle-resolved photoemission spectroscopy experiments that additionally found a pronounced quasiparticle weight at the zone center. Moreover, we observe a significant sensitivity of the bulk electronic structure of WTe_2 around the Fermi level to electronic correlations and renormalizations due to self-energy effects, previously neglected in first-principles descriptions.

DOI: 10.1103/PhysRevLett.119.026403

Introduction.—The observation of unconventional transport properties in WTe_2 [1], such as the large nonsaturating magnetoresistance with values among the highest ever reported, prompted experiments and theory to address the electronic structure of this semimetallic transition metal dichalcogenide (TMD) [2–6]. WTe_2 consists of layers of transition metal (TM) atoms sandwiched between two layers of chalcogen atoms, similarly to other TMDs such as MoS_2 and $MoSe_2$. Because of the layered structure, TMDs have commonly been considered as quasi-two-dimensional solids. The easiness of exfoliation down to a single layer makes them appealing for nanoscale electronic applications. WTe_2 has also been theoretically described, in a recent paper, as the prototypical system to host a new topological state of matter called a type-II Weyl semimetal [7]. At odds with standard type-I Weyl semimetals showing a pointlike Fermi surface, the type-II Weyl excitations arise at the contact between the hole and electron pockets. Theoretical predictions were immediately followed by several surface sensitive angle-resolved photoemission spectroscopy (ARPES) studies claiming evidence of topological Fermi arcs [8–10].

Our previous investigation by surface sensitive ARPES, spin-resolved ARPES, and DFT calculations, gave clear hints about the nonpurely two-dimensional (2D) electron states of WTe_2 and suggested interlayer, i.e., k-perpendicular (k_z) dispersion and cross-layer compensation of electrons and holes [11]. However, a direct inspection of the electronic properties by means of the bulk sensitive soft-x-ray ARPES technique, and more accurate calculations are needed in order to prove the three-dimensional (3D) character of the bulk electronic structure. By measuring ARPES with photon energy $h\nu$ in the range 400–800 eV, one probes the electron states averaging on several layers and therefore reducing the weight of the surface specific features that otherwise dominate the spectra when excitation energies in the VUV-range are employed. Furthermore, the increase of the photoelectron mean free path in the soft-x-ray energy range results in a high intrinsic k_z resolution of the ARPES experiment [12], which is essential to explore 3D effects in electronic band structure.

WTe_2 displays an unprecedentedly large nonsaturating magnetoresistance even at magnetic fields $\mathbf{B}$ as high as 60 T [1]. A large orbital magnetoresistance is expected in semimetals, so that WTe_2 shares this intriguing feature with bismuth and graphite [13], all showing small concentrations of very mobile hole and electron carriers. Differently from bismuth and graphite, however, the magnetoresistance in WTe_2 exactly follows a $\mathbf{B}^2$ dependence typical of an

electron-hole compensated semimetal [14]. Carrier compensation, in turn, is only a necessary condition. It is equally mandatory that the carrier mobility does not depend on the applied magnetic field, a feature met by WTe_2 [1], but not, for example, by pure bismuth [15]. The bulk electronic structure of WTe_2 has been so far only investigated by means of transport measurements [5,6]. The behavior of the resistivity under an external magnetic field is hard to reconcile with the picture of a layered solid: when the magnetic field is applied parallel to the layers, unexpected quantum oscillations were observed, suggesting that electrons may travel in a coherent way also across the weakly bonded layers [5]. Moreover, recent spin-ARPES data indicated both in-plane and out-of-plane spin polarization of the electron states below the Fermi level, deviating from what was expected from spin-orbit interaction (SOI) in a noninteracting 2D layered system [11], and the balance between the hole and electron states was shown to be fully established only if cooperation of several layers, i.e., bulk 3D character, was included [11]. The above results, albeit indirectly, suggest that the electronic structure of WTe_2 has an intrinsic 3D character, unexpectedly for a TMD. However, up to now, no conclusive spectroscopic evidence of three dimensionality was reported.

Results and discussion.—In Fig. 1(c) we report the k_z evolution of the Fermi surface spanning about 9 Brillouin zones in the out-of-plane reciprocal direction and about 3 in-plane Brillouin zones along the W chain direction k_x. Our measurements unambiguously unveil a clear continuous k_z dispersion of the electronic states at the Fermi level, definitely proving that WTe_2 has a 3D bulk electronic structure despite the layered geometry common to all TMDs [12], and despite the preferential direction for electronic dispersion given by the zigzag TM chains. These results provide a direct spectroscopic validation of the early proposals based on quantum oscillation experiments and temperature-dependent magnetoresistance measurements [5,6].

A closer look at the k_z evolution of the electronic states around $k_x = 0$ would suggest the out-of-plane periodicity be ~ 0.9 Å^{-1} [two rectangles along k_z in Fig. 1(c)], as resulting from a unit cell containing only one WTe_2 layer, and contrary to the experimental structure consisting of two layers, as depicted in Fig. 1(a) [16]. It is not unusual that the experimentally measured periodicity of a system does not match that of the structural unit cell. Common examples are given by nonsymmorphic systems such as CrO_2, graphite, and 2H-WSe_2 [17–19], for which selection rules restrict the final state symmetry. WTe_2 crystallizes in the nonsymmorphic space group $Pmn2_1$. The nonsymmorphicity ensures a symmetry protected band degeneracy at the Brillouin zone point $Z = (0, 0, \pi/c)$ [see Fig. 1(a) in the Supplemental Material [20]], despite that the fractional translation invariance along the k_z direction is broken by the nonequivalence of WTe_2 monolayers. To model this double periodicity in band structure calculations, we have projected the effective band structure of WTe_2 onto the irreducible representations of a Brillouin zone compatible with the one extracted from our experiments, with restored k_z fractional translation invariance [30–32]. We find indeed that the unfolded band structure, having relatively clean unfolded bands around

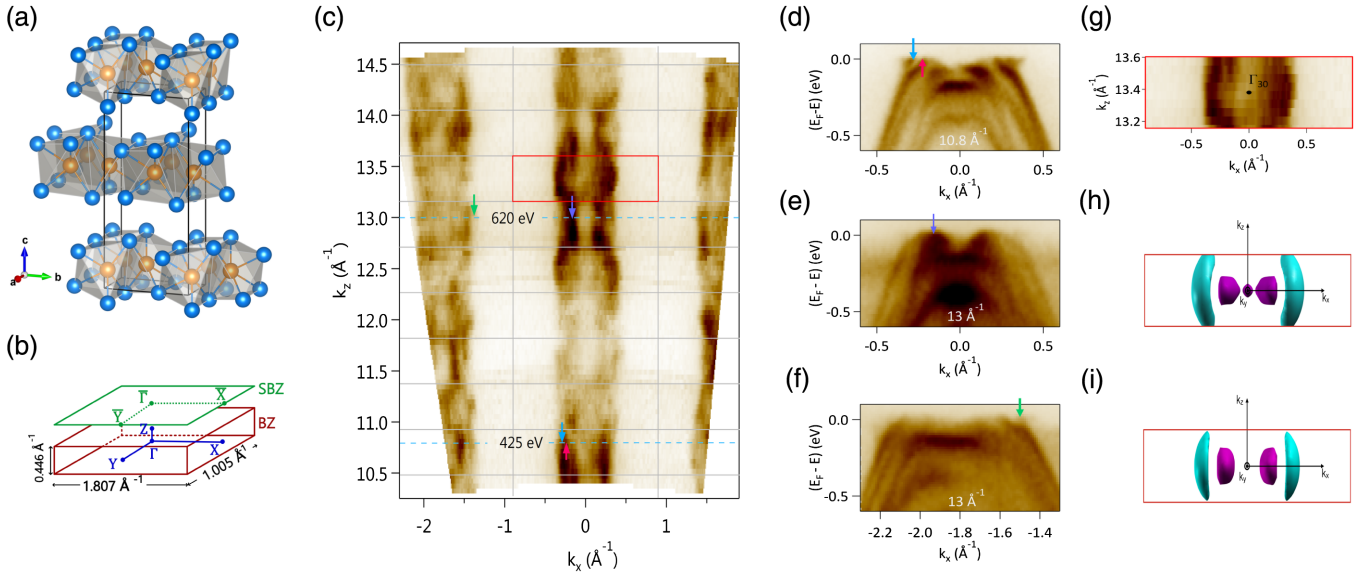

FIG. 1. (a) View of the WTe_2 crystal structure. W and Te atoms are shown in orange and blue, respectively. (b) Relative bulk and (001) surface Brillouin zones. (c) k_x-k_z Fermi surface ($k_y = 0$) taken in the 400–800 eV range of excitation energies. The value of the inner potential $V_0 = -6.5$ eV is used to compute the k_z periodicity over many Brillouin zones (see rectangles), assumed here to be $2\pi/c \sim 0.45$ Å^{-1}; see main text for a discussion. (d)–(f) E vs k band dispersions along the blue dashed lines in (c). Arrows are guides to the eyes to highlight features from the hole and electron pockets in a way consistent with (c). (g) Enlargement of the k_x-k_z Fermi surface around the Γ_{30} point [red rectangle in (c)], and (h)–(i) calculated Fermi surface within the LDA and LDA + U ($U = 2$ eV) approximations.

the Fermi level, explains the observed periodicity, as shown in the Supplemental Material, Fig. 1(b) [20].

The double k_z extent of the Fermi surface can be further inspected by a closer analysis of the electronic dispersions [33]. At the Fermi level, the spectrum in Fig. 1(d) shows the expected bulk hole and electron pockets along the k_x direction, as highlighted by the light blue and red arrows, respectively. On the other hand, the spectrum in Fig. 1(e), which misses such features at the Fermi level around $k_x = 0$, recovers the two pockets at the neighbor in-plane Brillouin zones around $k_x \sim \pm 1.8$ Å^{-1} [see Fig. 1(f)]. We, therefore, conclude that the measured intensities are strongly modified by matrix element effects, enhancing selectively electron and hole contributions in subsequent Brillouin zones.

A notable difference between present soft-x-ray data and VUV ones [see Fig. 2(a) and Refs. [11,34]] as well as laser excited ARPES [35] is the lack of any evident spectral intensity at the zone center Γ. Nevertheless, the observation of small frequency quantum oscillations suggests the presence of tiny electron pockets at both sides of, and almost touching at, the Γ point [5,35]. Our measured Fermi surface reports no clear evidence of these type of structures

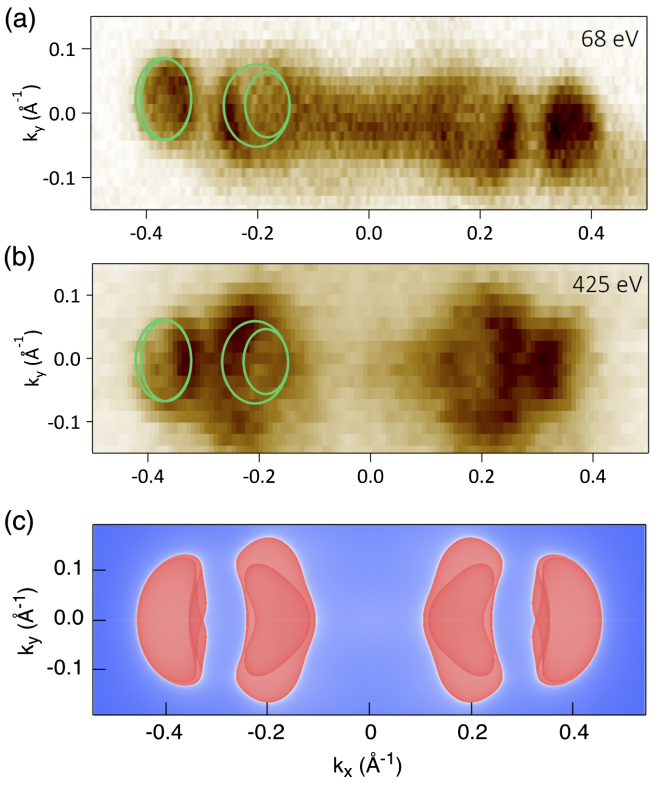

FIG. 2. k_x-k_y Fermi surfaces recorded with (a) UV ARPES at $h\nu = 68$ eV ($k_z = 4.3$ Å^{-1}) and (b) soft-x-ray ARPES at $h\nu = 425$ eV ($k_z = 10.8$ Å^{-1}), respectively. Green solid lines are reproduced from Ref. [35], corresponding to the extremal orbits with the areas determined from quantum oscillation measurements. (c) Calculated k_x-k_y bulk Fermi surface within the LDA + U approximation for $U = 2$ eV.

[see Fig. 2(b) of the main text and Fig. 2 of the Supplemental Material [20]]. In Figs. 2(a) and 2(b) we also highlight, by means of solid green circles, the extension of extremal orbits corresponding to given frequencies in quantum oscillation measurements [35]. While such extensions, approximately of equal size (~0.025 Å^{-2}) for both pockets, fit with our UV ARPES Fermi surface, bulk sensitive soft-x-ray ARPES shows that the dimension of the hole pocket is much larger than estimated [36]. Since the observed area of the two pockets differ on the $k_z \sim 0$ plane, in this respect, our results establish that the 3D dispersion of the Fermi surface is crucial for the electron-hole compensation that in turn explains the reported giant magnetoresistance. This is also in line with recent magnetotransport experiments, supporting the need of three-dimensionality for having such an extremely large effect [37].

The measured electron pocket is characterized by a bowlike k_z dispersion [Fig. 1(g)], in agreement with the calculated Fermi surface based on the local density approximation (LDA) plus an on-site Hubbard U of 2 eV (compare with cyan areas in Fig. 1(i). However, discrepancies arise when comparing the hole pocket dispersion. In the measured Fermi surface, hole pockets seem to disperse all over the k_z extension of the Brillouin zone, while first-principles calculations give disconnected pockets [purple areas in Fig. 1(i)]. However, it is worth noting that the calculated k_x-k_y Fermi surface [Fig. 2(c)], nicely reproduces the features and the extensions of the measured Fermi surface. This improves over standard (i.e., without U) LDA calculations [see Fig. 1(h), discussions in Refs. [2,5,11], and discussion below], suggesting that electronic correlation could play a significant role. In fact, previous theoretical studies have demonstrated that LDA is capable of providing an overall good description of the electronic structure of WTe_2, especially the coexistence of electron and hole features and the onset of topological surface states, but at a quantitative level, significant discrepancies with experiment remain. In particular, LDA tends to overestimate the dimensions of the Fermi surface along the W chains direction [see Fig. 1(h)], positioning the minimum of the electron pocket at momentum values larger than ARPES [11]. This, together with the difficulty in resolving tiny features dispersing around the Fermi level, has limited so far the understanding of surface and bulk contributions on the Fermi surface. Moreover, since calculations predict Weyl points to be above the Fermi level, a direct comparison with experiment requires an accurate treatment of the unoccupied states.

Despite the fairly delocalized character of 5d W orbitals, the inclusion of a moderate U in LDA leads to a sizable modification of the electronic states in the proximity of the Fermi level, as shown in Fig. 3. The general trend as a function of increasing U (see Fig. 4 of the Supplemental Material [20] for more values) is the small shift of the electron pocket toward lower momentum values and the

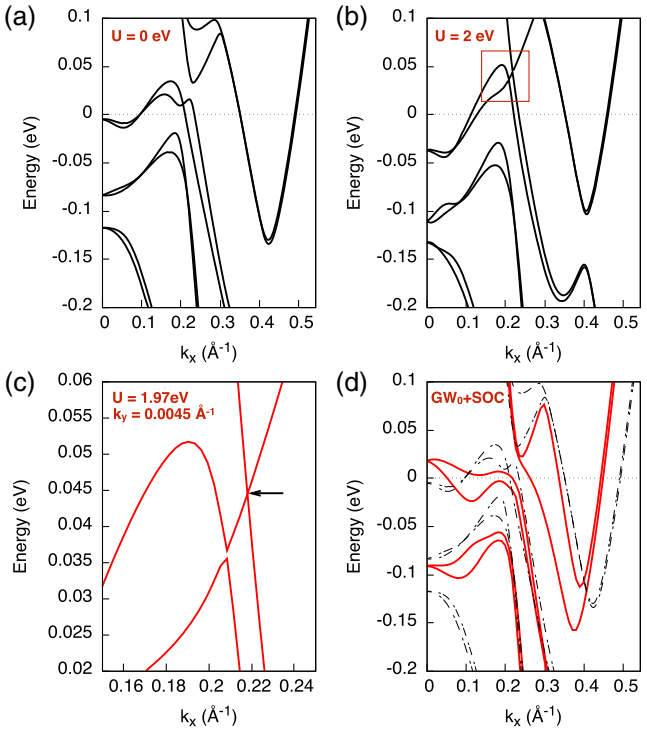

FIG. 3. (a)–(b) LDA + U band structures for $U = 0.0$ and 2.0 eV along the k_x direction, respectively. The red box in panel (b) refers to the zoom area in (c) where the 3D linear band crossing (see arrow) occurs at finite $k_y = \pm 0.0045$ Å^{-1} for U values smaller than the critical $U_c = 1.98$ eV. (d) GW band structure (solid red) as compared to the LDA (dot-dashed black).

sizable modification of the hole pocket. It is interesting to note how for $U = 2$ eV, the value that gives a nice comparison between measured and calculated Fermi surfaces as shown in Fig. 2, the two pockets almost linearly cross at ~50 meV above the Fermi level along the k_x direction. A further increase of the U (Fig. 4 of the Supplemental Material [20]) causes the reopening of the gap between these pockets. If this correlation driven trend leads to a change of the topological properties of WTe_2 it would deserve a proper investigation. What we highlight here is that for U values slightly smaller than 2 eV, bands linearly cross at finite k_y, symmetric with respect the k_x axis, giving rise to type-I Weyl points, as shown in Fig. 3(c). Such Weyl points, having opposite chirality, are connected by Fermi arcs when projected onto the surface Brillouin zone (Fig. 5 of the Supplemental Material [20]). At the critical value $U_c = 1.98$ eV these Weyl points touch on the k_x axis and annihilate. The appearance of a type-I Weyl point has been suggested as the fingerprint of topological transitions in noncentrosymmetric topological insulators [38]. Despite the approximate way in which DFT+U treats the electron-electron interaction, i.e., within an energy independent Hartree approximation, the improved description of the Fermi surface both in the $k_x - k_y$ plane and in the k_z direction, as well as of the optical conductivity of WTe_2 (Fig. 6 of the Supplemental Material [20]), indicates that the electronic states experience a non-negligible degree of correlation.

To fully endorse this thesis, we perform GW calculations in which band renormalization is induced by truly many-body self-energy effects. The resulting band structure, obtained within a relativistic framework, is shown in Fig. 3(d). It displays significant changes with respect to the underlying DFT (dotted-dashed lines) and DFT + U ones: the position of the electron pockets shifts closer to the Γ point, in better agreement with ARPES experiments, but in contrast to DFT(+U), GW finds a density of empty states at Γ right above the Fermi level, which leads to a strong renormalization of the hole pocket; finally, the quasiparticle bands exhibit a larger SOI induced splitting, which could indicate a strong coupling between relativistic effects and electronic correlations, a novel quantum phenomenon recently observed in other heavy materials subjected to Lifshitz-type instabilities [39]. Remarkably, our GW results may explain the observed large spin polarization and complex spin texture recently reported in Ref. [11], hardly reconcilable with standard DFT calculations.

Concluding remarks.—In this Letter, we address the bulk electronic properties of WTe_2 by complementary bulk-sensitive electron spectroscopy and theoretical methods. Since the prediction of topological surface states in WTe_2 owing to a topological nature and its classification as type-II Weyl semimetal, the spectroscopic study of the bulk electronic structure of WTe_2 was missing. Our soft-x-ray ARPES measurements, by means of an unprecedentedly high intrinsic definition of k_z and a large range of its variation in the Fermi surface mapping, definitely demonstrate a 3D character of the electronic states. These results prove that layered materials such as TMDs host electrons moving from layer to layer in a coherent way, in agreement with the quantum oscillation transport experiments [5], at odds with TMD monolayers, recently proposed to host quantum spin Hall physics [40]. Moreover, our theoretical investigation sheds light on the role of electronic correlations and self-energy effects on those electronic states, dispersing around the Fermi level, which play a relevant role in the transport properties of WTe_2.

D. D. S., G. S., and R. T. acknowledge the German Research Foundation (DFG-SFB 1170 Tocotronics), ERC-StG-336012-Thomale-TOPOLECTRICS, NSF PHY-1125915 and the SuperMUC system at the Leibniz Supercomputing Centre under the Project-ID pr94vu. The soft-x-ray ARPES experiment was carried out at the ADRESS beam line [41,42] at the Swiss Light Source, Paul Scherrer Institute, Switzerland. UV-ARPES experiment was performed at APE-IOM beam line at the Elettra-Sincrotrone Trieste facility (Italy) [43]. The work at CNR-SPIN and CNR-IOM was performed within the framework of the nanoscience foundry and fine analysis (NFFA-MIUR Italy) project. The research in Vienna was

supported by the Austrian Science Fund (Grant No. I1490-N19). Computing time at the Vienna Scientific Cluster (VSC3) is gratefully acknowledged. The research at Princeton was supported by the US NSF MRSEC Program Grant No. DMR-1420541. J. A. K. was supported by the Swiss National Science Foundation (SNF-Grant No. 200021-165910).

P. K. D. and D. D. S. contributed equally to this work.

*domenico.disante@physik.uni-wuerzburg.de
†Present address: Singapore Synchrotron Light Source, National University of Singapore, 5 Research Link, Singapore 117603.
das@nus.edu.sg

[1] M. N. Ali, J. Xiong, S. Flynn, J. Tao, Q. D. Gibson, L. M. Schoop, T. Liang, N. Haldolaarachchige, M. Hirschberger, N. P. Ong *et al.*, Nature (London) **514**, 205 (2014).
[2] I. Pletikosić, M. N. Ali, A. V. Fedorov, R. J. Cava, and T. Valla, Phys. Rev. Lett. **113**, 216601 (2014).
[3] J. Jiang, F. Tang, X. C. Pan, H. M. Liu, X. H. Niu, Y. X. Wang, D. F. Xu, H. F. Yang, B. P. Xie, F. Q. Song *et al.*, Phys. Rev. Lett. **115**, 166601 (2015).
[4] Y. Wu, N. H. Jo, M. Ochi, L. Huang, D. Mou, S. L. Bud'ko, P. C. Canfield, N. Trivedi, R. Arita, and A. Kaminski, Phys. Rev. Lett. **115**, 166602 (2015).
[5] Z. Zhu, X. Lin, J. Liu, B. Fauqué, Q. Tao, C. Yang, Y. Shi, and K. Behnia, Phys. Rev. Lett. **114**, 176601 (2015).
[6] L. R. Thoutam, Y. L. Wang, Z. L. Xiao, S. Das, A. Luican-Mayer, R. Divan, G. W. Crabtree, and W. K. Kwok, Phys. Rev. Lett. **115**, 046602 (2015).
[7] A. A. Soluyanov, D. Gresch, Z. Wang, Q. Wu, M. Troyer, X. Dai, and B. A. Bernevig, Nature (London) **527**, 495 (2015).
[8] F. Y. Bruno, A. Tamai, Q. S. Wu, I. Cucchi, C. Barreteau, A. de la Torre, S. McKeown Walker, S. Riccò, Z. Wang, T. K. Kim *et al.*, Phys. Rev. B **94**, 121112 (2016).
[9] C. Wang, Y. Zhang, J. Huang, S. Nie, G. Liu, A. Liang, Y. Zhang, B. Shen, J. Liu, C. Hu *et al.*, Phys. Rev. B **94**, 241119 (2016).
[10] Y. Wu, D. Mou, N. H. Jo, K. Sun, L. Huang, S. L. Bud'ko, P. C. Canfield, and A. Kaminski, Phys. Rev. B **94**, 121113 (2016).
[11] P. K. Das, D. Di Sante, I. Vobornik, J. Fujii, T. Okuda, E. Bruyer, A. Gyenis, B. E. Feldman, J. Tao, R. Ciancio *et al.*, Nat. Commun. **7**, 10847 (2016).
[12] V. N. Strocov, M. Shi, M. Kobayashi, C. Monney, X. Wang, J. Krempasky, T. Schmitt, L. Patthey, H. Berger, and P. Blaha, Phys. Rev. Lett. **109**, 086401 (2012).
[13] X. Du, S.-W. Tsai, D. L. Maslov, and A. F. Hebard, Phys. Rev. Lett. **94**, 166601 (2005).
[14] A. B. Pippard, *Magnetoresistance in Metals* (Cambridge University Press, Cambridge, England, 1989).
[15] A. Collaudin, B. Fauqué, Y. Fuseya, W. Kang, and K. Behnia, Phys. Rev. X **5**, 021022 (2015).
[16] A. Mar, S. Jobic, and A. Ibers, J. Am. Chem. Soc. **114**, 8963 (1992).
[17] F. Bisti, V. A. Rogalev, M. Karolak, S. Paul, A. Gupta, T. Schmitt, G. Güntherodt, G. Sangiovanni, G. Profeta, and V. N. Strocov, arXiv:1607.01703.
[18] D. Pescia, A. R. Law, M. T. Johnson, and H. P. Hughes, Solid State Commun. **56**, 809 (1985).
[19] T. Finteis, M. Hengsberger, T. Straub, K. Fauth, R. Claessen, P. Auer, P. Steiner, S. Hüfner, P. Blaha, M. Vögt *et al.*, Phys. Rev. B **55**, 10400 (1997).
[20] See Supplemental Material at http://link.aps.org/supplemental/10.1103/PhysRevLett.119.026403 for experimental and computational details, as well as additional ARPES spectra and calculations. which includes Refs. [16,21–29].
[21] G. Kresse and J. Furthmüller, Phys. Rev. B **54**, 11169 (1996).
[22] G. Kresse and D. Joubert, Phys. Rev. B **59**, 1758 (1999).
[23] J. P. Perdew, K. Burke, and M. Ernzerhof, Phys. Rev. Lett. **77**, 3865 (1996).
[24] S. L. Dudarev, G. A. Botton, S. Y. Savrasov, C. J. Humphreys, and A. P. Sutton, Phys. Rev. B **57**, 1505 (1998).
[25] L. Hedin, Phys. Rev. **139**, A796 (1965).
[26] M. Shishkin and G. Kresse, Phys. Rev. B **74**, 035101 (2006).
[27] A. A. Mostofi, J. R. Yates, Y.-S. Lee, I. Souza, D. Vanderbilt, and N. Marzari, Comput. Phys. Commun. **178**, 685 (2008).
[28] C. Franchini, R. Kováčik, M. Marsman, S. Sathyanarayana Murthy, J. He, C. Ederer, and G. Kresse, J. Phys. Condens. Matter **24**, 235602 (2012).
[29] C. C. Homes, M. N. Ali, and R. J. Cava, Phys. Rev. B **92**, 161109 (2015).
[30] M. Tomić, H. O. Jeschke, and R. Valentí, Phys. Rev. B **90**, 195121 (2014).
[31] W. Ku, T. Berlijn, and C.-C. Lee, Phys. Rev. Lett. **104**, 216401 (2010).
[32] V. Popescu and A. Zunger, Phys. Rev. Lett. **104**, 236403 (2010).
[33] Spectra in Figs. 1(d),1(e), and 1(f) refer to photon energies $h\nu = 425$ and 620 eV, such that Fermi surfaces in the first in-plane Brillouin zone ($k_x \sim 0$) look different (see $k_z = 10.8$ Å^{-1} and $k_z = 13.0$ Å^{-1} in Fig. 1(c). Spectra for $h\nu = 425$, 570 eV ($k_z = 12.5$ Å^{-1}) and 668 eV ($k_z = 13.4$ Å^{-1}) are similar.
[34] J. Jiang, F. Tang, X. C. Pan, H. M. Liu, X. H. Niu, Y. X. Wang, D. F. Xu, H. F. Yang, B. P. Xie, F. Q. Song *et al.*, Phys. Rev. Lett. **115**, 166601 (2015).
[35] Y. Wu, N. H. Jo, D. Mou, L. Huang, S. L. Budko, P. C. Canfield, and A. Kaminski, Phys. Rev. B **95**, 195138 (2017).
[36] We note here that the observed increment in the size of the hole pocket using soft x ray is not a consequence of the cross-section variations of Te $5p$ and W $5d$ orbitals as both of them are decreasing almost in the same manner from UV to the energy ranges used in the present study.
[37] J. Na, A. Hoyer, L. Schoop, D. Weber, B. V. Lotsch, M. Burghard, and K. Kern, Nanoscale **8**, 18703 (2016).
[38] J. Liu and D. Vanderbilt, Phys. Rev. B **90**, 155316 (2014).

Supplemental Material: Three-Dimensional Electronic Structure of type-II Weyl Semimetal WTe_2

D. Di Sante,[1] P. K. Das,[2,3] C. Bigi,[4] Z. Ergönenc,[5] N. Gürtler,[5] J. A. Krieger,[6,7] T. Schmitt,[8] M. N. Ali,[9] G. Rossi,[4] R. Thomale,[1] C. Franchini,[5] S. Picozzi,[10] J. Fujii,[2] V. N. Strocov,[8] G. Sangiovanni,[1] I. Vobornik,[2] R. J. Cava,[9] and G. Panaccione[2]

[1]*Institut für Theoretische Physik und Astrophysik, Universität Würzburg, Am Hubland Campus Süd, Würzburg 97074, Germany**
[2]*Istituto Officina dei Materiali (IOM)-CNR, Laboratorio TASC, in Area Science Park, S.S.14, Km 163.5, I-34149 Trieste, Italy*†
[3]*International Centre for Theoretical Physics (ICTP), Strada Costiera 11, I-34100 Trieste, Italy*
[4]*Dipartimento di Fisica, Universitá di Milano, Via Celoria 16, I-20133 Milano, Italy*
[5]*Computational Materials Physics, University of Vienna, Sensengasse 8/8, A-1090 Vienna, Austria*
[6]*Laboratory for Muon-Spin Spectroscopy, Paul Scherrer Institute, CH-5232 Villigen, Switzerland*
[7]*Laboratorium für Festkörperphysik, ETH-Hönggerberg, CH-8093 Zürich, Switzerland*
[8]*Paul Scherrer Institute, Swiss Light Source, CH-5232 Villigen, Switzerland*
[9]*Department of Chemistry, Princeton University, Princeton, New Jersey 08544, USA*
[10]*Consiglio Nazionale delle Ricerche (CNR-SPIN), Via Vetoio, L'Aquila 67100, Italy*

(Dated: April 25, 2017)

METHODS

Soft X-ray ARPES measurements were performed at ADRESS beamline at Swiss Light Source (Villigen, Switzerland) using Specs analyzer with an energy resolution better than 40 meV and angular resolution better than 0.1 deg. The photon energy used is in the range of 300 eV to 800 eV. The band dispersion along the direction k_z perpendicular to surface is probed by means of photon energy dependent measurements, while the two-dimensional Fermi surface (k_x-k_y) mapping was obtained by tilting the sample perpendicularly to the slit direction in steps of 0.2 deg (with $\sim$ 100 meV of energy resolution). WTe_2 single crystals were cleaved inside UHV. Measurements were performed under a vacuum better than 5×10^{-11} mbar, and at temperature of 6 K. UV-ARPES experiments were performed at APE-IOM low energy beamline at the Elettra-Sincrotrone Trieste facility (Italy), by using a Scienta DA30 analyzer with energy resolution better than 10 meV and angular resolution better than 0.05 deg. with photon energy in the range 20-100 eV.

Density functional theory based calculations were performed by using the VASP ab-initio simulation package [1, 2]. Consistently with previous theoretical reports, the local density approximation within the PBE parametrization for the exchange-correlation potential was used, by expanding the Kohn-Sham wavefunction into plane-waves up to an energy cut-off of 400 eV [3]. Brillouin zone has been sampled on a $24\times12\times4$ regular mesh. SOC has been included self-consistently. Moreover, to go beyond the single particle picture, different level of sophistications were used, from LDA+U to treat electronic correlations within a energy independent Hartree description [4], up to state of the art GW calculations in order to include an explicit evaluation of the self-energy [5]. In this latter case, an accurate quasiparticle electronic structure was obtained by using a partially self-consistent GW_0 procedure including spin-orbit coupling[6], where we have updated the eigenvalues by iterating the Greens function G while keeping the screening properties W_0 constant at the DFT level. Convergence has been achieved by including about 2000 empty states on a Γ-centered $6\times6\times4$ **k**-mesh. This set-up guarantee converged quasiparticle energy with an accuracy of 5-10 meV. GW bandstructure were obtained by means of wannier function interpolation using the wannier90 suite [7] and the VASP2WANNIER90 interface [8]. For the construction of the localized wannier functions we have used projections on W s,d and Te s,p states. Atomic positions of WTe_2 were fully relaxed starting from experimental data in Ref. [9].

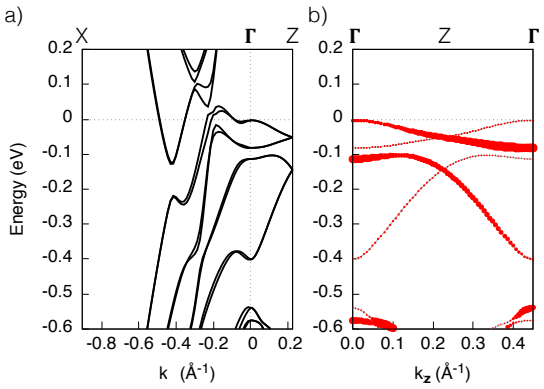

FIG. 1: **Bands folding.** a) DFT bandstructure along the X - Γ - Z direction. b) Bandstructure along k_z across 2 consecutive Brillouin zones. Red circles refer to weights resulting from the band unfolding procedure. A large intensity reduction for the bands folding back is observed.

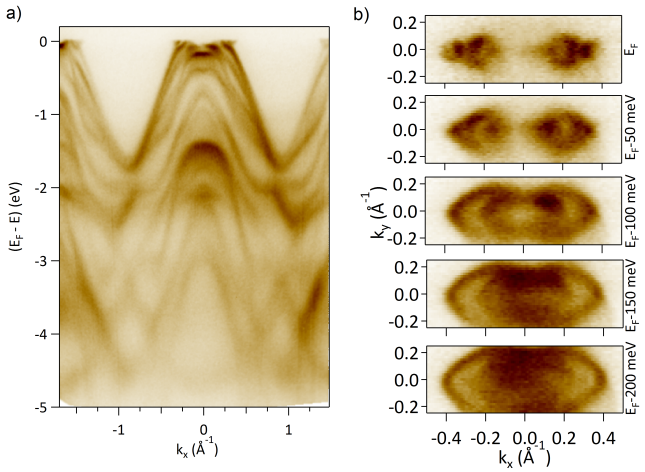

FIG. 2: **Deep valence band dispersion and constant energy cuts.** a) Band dispersion along $\Gamma - X$ direction is shown for wide binding energy ranges. The spectra are measured using photon energy value of 425 eV. Panel b) shows the constant energy cuts in the k_x-k_y plane at Fermi energy (top), and every 50 meV below down to 200 meV (bottom panel). This Fermi surface mapping was done using fixed photon energy value of 425 eV. Unlike our previous UV ARPES and other laser ARPES data, we have very little spectral intensity at the zone center (Γ) even at 100 meV below the Fermi energy while using soft-X ray.

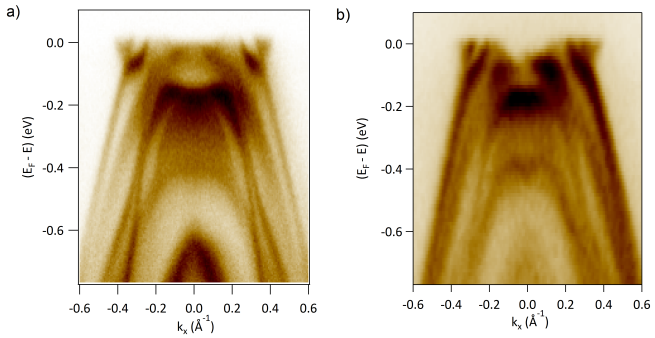

FIG. 3: **Comparison of band dispersion between UV ARPES data and soft-X ray ARPES data**. a) Band dispersion along $\Gamma - X$ direction measured using photon energy 68 eV, b) band dispersion measured using photon energy 425 eV.

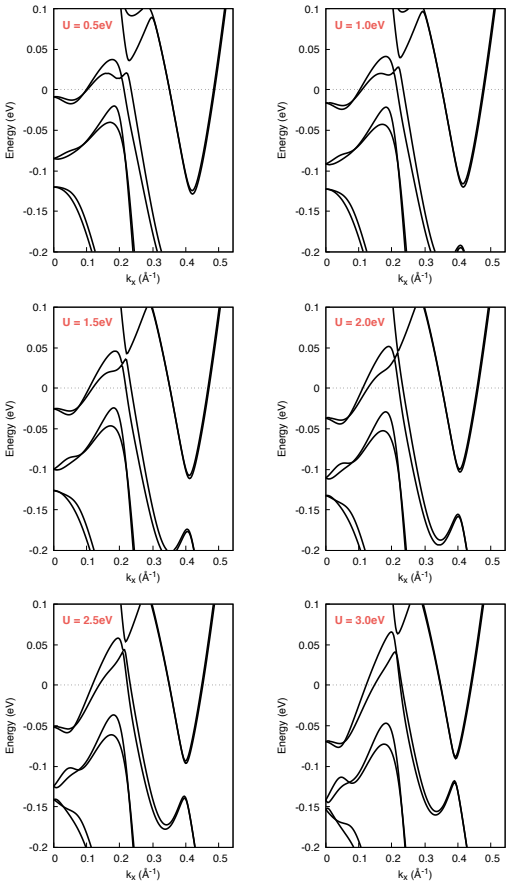

FIG. 4: **LDA+U band structure along the $\Gamma - X$ direction.** From top to bottom U = 0.5 eV, 1.0 eV, 1.5 eV, 2.0 eV, 2.5 eV, 3.0 eV.

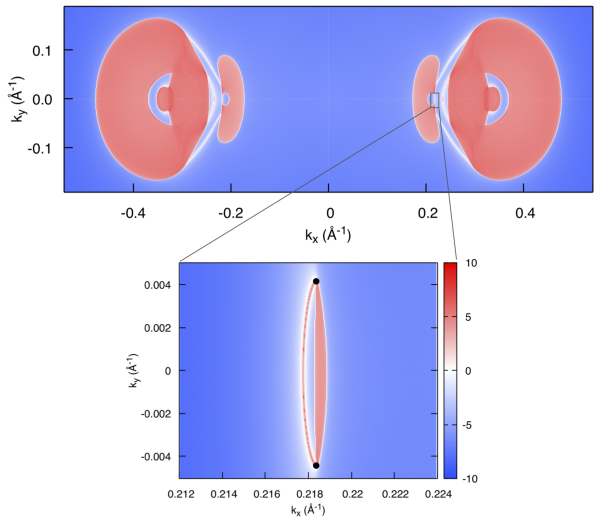

FIG. 5: **Fermi Arcs.** top panel) [001] surface Fermi Surface at the type-I Weyl point energy for a LDA+U calculation (at U = 1.97 eV). Fermi arcs connecting hole and electron pockets are clearly visible. bottom panel) zoom around the projected type-I Weyl points connected by a Fermi arc.

OPTICAL CONDUCTIVITY AND ELECTRON-ELECTRON INTERACTION

The theoretical ab-initio spectrum has been obtained from the following Kubo-Greenwood formula:

$$\sigma_{ij}(\omega) = \frac{\hbar e^2}{iVN_k}\sum_{n\neq m}\sum_{\mathbf{k}}\frac{f(\varepsilon_n)}{\varepsilon_m-\varepsilon_n} \times\left(\frac{v_{i,nm}v_{j,mn}}{\varepsilon_m-\varepsilon_n-\hbar\omega}-\frac{v_{j,nm}v_{i,mn}}{\varepsilon_m-\varepsilon_n+\hbar\omega}\right), \quad (1)$$

where $\sigma_{ij}(\omega)$ is the non-Drude part optical conductivity, $f(\varepsilon_n)$ is the Fermi-Dirac distribution function, and $\varepsilon_n = \varepsilon_n(\mathbf{k})$ and $|n(\mathbf{k})\rangle$ indicate the nth-eigenvalue and the corresponding eigenvector. In practical calculations, the energy $\hbar\omega$ is replaced by $\hbar\omega + i\delta$ in order to take into account the effect of carrier lifetime. Here, δ is assumed to be constant and equal to ~ 1 meV. The velocity matrix elements $v_{i,nm}$ are defined as

$$v_{i,nm} = \langle n|v_i(\mathbf{k})|m\rangle = \frac{1}{\hbar}\langle n|\frac{\partial H(\mathbf{k})}{\partial k_i}|m\rangle\,, \quad (2)$$

and are computed by downfolding the DFT+U ab-initio Hamiltonian $H(\mathbf{k})$ to an effective low-energy tight-binding model using maximally localized Wannier functions (see also Methods section). The Brillouin zone integration has been performed on a regular $N_k = 112\times112\times112$ k-point mesh. The DFT+U optical conductivity, with U $= 2$ eV, nicely reproduces the main features of the measured spectrum, including the peak at around 60 meV (~ 500 cm^{-1}) missing in standard DFT calculations as discussed in Ref. [10]. Moreover, the shoulder at 150 meV (1400 cm^{-1}) as well as the infrared peak at 20 meV (160 cm^{-1}) are better positioned compared to the experimental data than for the DFT spectrum.

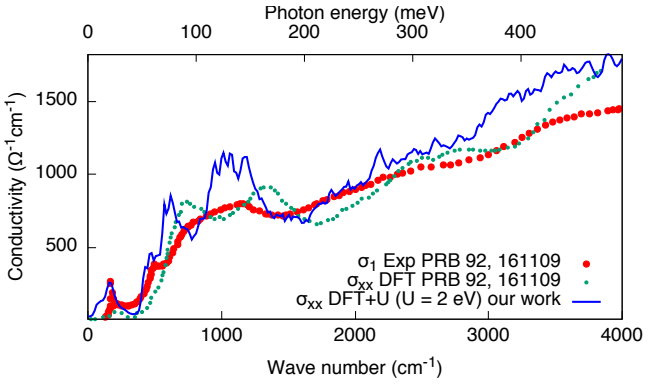

FIG. 6: **Optical Conductivity.** WTe_2 measured and calculated optical conductivity. Experimental and theoretical data for standard DFT, i.e. without U, have been reproduced from Ref. [10].

* Electronic address: domenico.disante@physik.uni-wuerzburg.de
† Electronic address: das@iom.cnr.it

[1] G. Kresse and J. Furthmüller, Phys. Rev. B **54**, 11169 (1996).
[2] G. Kresse and D. Joubert, Phys. Rev. B **59**, 1759 (1999).
[3] J. P. Perdew, K. Burke, and M. Ernzerhof, Phys. Rev. Lett. **77**, 3865 (1996).
[4] S. L. Dudarev, G. A. Botton, S. Y. Savrasov, C. J. Humphreys, and A. P. Sutton, Phys. Rev. B **57**, 1505 (1998).
[5] L. Hedin, Phys. Rev. **139**, A796 (1965).
[6] M. Shishkin and G. Kresse, Phys. Rev. B **74**, 035101 (2006).
[7] A. A. Mostofi, J. R. Yates, Y.-S. Lee, I. Souza, D. Vanderbilt, and N. Marzari, Comput. Phys. Commun. **178**, 685 (2008).
[8] C. Franchini, R. Kováčik, M. Marsman, S. Sathyanarayana Murthy, J. He, C. Ederer, and G. Kresse, J. Phys. Condens. Matter. **24**, 235602 (2012).
[9] A. Mar, S. Jobic, and A. Ibers, J. Am. Chem. Soc. **114**, 8963 (1992).
[10] C. C. Homes, M. N. Ali, and R. J. Cava, Phys. Rev. B **92**, 161109 (2015).

[39] B. Kim, P. Liu, Z. Ergönenc, A. Toschi, S. Khmelevskyi, and C. Franchini, Phys. Rev. B **94**, 241113 (2016).

[40] S. Tang *et al.*, Nat. Phys. **13**, 683 (2017).

[41] V. N. Strocov, T. Schmitt, U. Flechsig, T. Schmidt, A. Imhof, Q. Chen, J. Raabe, R. Betemps, D. Zimoch, J. Krempasky *et al.*, J. Synchrotron Radiat. **17**, 631 (2010).

[42] V. N. Strocov, X. Wang, M. Shi, M. Kobayashi, J. Krempasky, C. Hess, T. Schmitt, and L. Patthey, J. Synchrotron Radiat. **21**, 32 (2014).

[43] G. Panaccione, I. Vobornik, J. Fujii, D. Krizmancic, E. Annese, L. Giovanelli, F. Maccherozzi, F. Salvador, A. D. Luisa, D. Benedetti *et al.*, Rev. Sci. Instrum. **80**, 043105 (2009).